Chemical Engineering Journal 372 (2019) 341–351

Contents lists available at ScienceDirect

Chemical Engineering Journal

journal homepage: www.elsevier.com/locate/cej

Effective chromium removal from water by polyaniline-coated electrospun adsorbent membrane

Guilherme Dognani[a,b,*], Pejman Hadi[b,c], Hongyang Ma[b,d], Flavio C. Cabrera[a], Aldo E. Job[a], Deuber L.S. Agostini[a], Benjamin S. Hsiao[b,*]

[a] School of Technology and Sciences, São Paulo State University (UNESP), Presidente Prudente, SP 19060-900, Brazil
[b] Department of Chemistry, Stony Brook University, Stony Brook, NY 11794, USA
[c] New York State Center for Clean Water Technology, Stony Brook University, NY 11794, USA
[d] State Key Laboratory of Organic-Inorganic Composites, Beijing University of Chemical Technology, Beijing 100029, China

HIGHLIGHTS

- Polyaniline-coated PVDF-HFP nanofibrous membranes were fabricated.
- Chromium was effectively removed from wastewater using the adsorbent membranes.
- Cr(VI) was first adsorbed on the imine groups and then reduced to Cr(III).
- PAni-coated membranes were successfully recycled and reused for at least 5 cycles.

ARTICLE INFO

Keywords:
Adsorbent membrane
Chromium removal
Polyaniline
Adsorption
Electrospinning
Nanofibers

ABSTRACT

Polyaniline (PAni)-coated polyvinylidenefluoride-co-hexafluoropropilene (PVDF-HFP) nanofibrous membranes were fabricated by electrospinning of PVDF-HFP followed by *in-situ* polymerization of PAni on the nanofiber surface. The resulting membranes with PAni coating were applied for chromium removal, where the efficiency was evaluated as functions of the pH value and adsorption time. Dynamic adsorption tests were also carried out at different flow rates and volumes of chromium in water. It was found that the PAni coating greatly enhanced the chromium removal efficiency with the maximum adsorption capacity being 15.08 mg/g at pH = 4.5. The desorption study further confirmed the recyclability of the PAni coated PVDF-HFP membrane showing an efficiency over 70% even after 5 cycles of usage. The structure and property relationships of these membranes were also characterized by FTIR spectroscopy, capillary flow porometer, water contact angle, scanning electron microscopy and X-ray photoelectron spectroscopy.

1. Introduction

Although the incessant quest for the development of new materials, processes and applications in the society has greatly improved the quality of our daily life [1], this progress has also led to serious environmental pollution problems due to the ever-increasing use of some toxic compounds. These compounds, although an indispensable part of the industrial progress, can bring about catastrophic challenges if not dealt with correctly. Among them, chromium is one of the widely-used elements in industrial processes, such as metal finishing, textile dyeing, plating, pigments, batteries, leather tanning, etc [2–4]. The World Health Organization (WHO) has recommended that the maximum allowable concentration for the total chromium concentration in drinking water should be less than 0.05 mg/L [5,6]. Chromium typically exists in the natural environment in two oxidation states: hexavalent Cr(VI) and trivalent Cr(III). The less toxic trivalent form (Cr(III)) is an essential nutrient for human life, which is also a more stable oxidation state in the environment. However, Cr(VI) is highly toxic, and is very soluble and thus quite mobile in groundwater and surface water [7–10]. The most common form of Cr(VI) has been the dichromate ion ($Cr_2O_7^{2-}$), a compound well-known for its severe noxious effects on human health [11].

To minimize the risk of environmental impacts to humans, Cr(VI) should be removed from the water body. Among the current methods for removal of chromium, adsorption has been considered as the most widely used techniques due to its low-cost, high regeneration ability

* Corresponding author at: School of Technology and Sciences, São Paulo State University (UNESP), Presidente Prudente, SP 19060-900, Brazil.
E-mail addresses: dognani.g@gmail.com (G. Dognani), pejman.hadimyavagh@stonybrook.edu (P. Hadi), benjamin.hsiao@stonybrook.edu (B.S. Hsiao).

https://doi.org/10.1016/j.cej.2019.04.154
Received 24 December 2018; Received in revised form 19 April 2019; Accepted 22 April 2019
Available online 22 April 2019
1385-8947/

and high efficiency [11–13]. In the wide spectrum of sorptive materials, conductive polymers have received a good deal of attention due to their efficiency. In particular, polyaniline (PAni) has been considered as a good candidate material because of its facile synthesis, relatively low-cost and environmental stability [14,15]. Many polyaniline-based composites, containing polyacrylonitrile nanofibers [10], silica gel [13], polystyrene nanofibers [14], MnO_2/TiO_2 [16], folic acid [17], ethyl cellulose [18], clay minerals [19], chitosan gel [8] and jute fibers, have been demonstrated for chromium reduction and removal [20]. The amine and imine groups on the polyaniline structure can act as electron donors for the reduction of Cr(VI) to Cr(III). In other words, these sites offer both chelating and adsorbent functions, where Cr(VI) is first reduced into Cr (III) and then adsorbed on the polyaniline surface [17,21]. In addition, the chromium reduction can cause an electron transfer onto the polyaniline chain and change its oxidation state from the emeraldine form to the pernigraniline form (i.e., a higher oxidation state of PAni) [20,22]. However, the polyaniline component can generally aggregate in solution, resulting in less surface area and lower adsorption capacity for chromium removal. Since the electrospinning technique can produce nanofibrous scaffolds with large surface areas and high porosities, the goal of the present study was to demonstrate that the combination of polyaniline and highly porous electrospun scaffolds could provide highly permeable nanofibrous membrane with good adsorption capability that would overcome the agglomeration of polyaniline chains and its surface area reduction problems.

In this study, a nanofibrous scaffold based on PVDF-HFP, a polymer with excellent chemical and thermal stability [23–25] was first produced by electrospinning and used as the substrate to prepare a composite membrane with dual filtration and adsorption capabilities. In specific, the electrospun PVDF-HFP nanofibrous scaffold was coated by polyaniline (PAni) through *in-situ* polymerization of aniline. The coated polyaniline surface was found to function as an adsorbent to remove Cr (VI) from water. Both static and dynamic adsorption performances of Cr (VI) of the polyaniline-coated PVDF-HFP membranes was evaluated. The Cr(VI) adsorption capacities of these membranes at various operating conditions were also investigated, where the membranes were further characterized by FTIR spectroscopy, capillary flow porometer, water contact angle, scanning electron microscopy (SEM) and X-ray photoelectron spectroscopy.

2. Experimental

2.1. Chemicals and materials

Poly(vinylidinefluoride-co-hexafluoropropylene) (PVDF-HFP), Kynar Flex 2821-00®, was provided by Arkema Brazil Inc. N,N-dimethylformamide (DMF, ACS reagent), acetone (ACS reagent), aniline (ACS-grade) and 1,5-Dyphenilcarbazide (ACS-grade) were purchased from Fisher Scientific. ACS-grade ammonium peroxidodisulfate (APS) and 5-sulfosalicylic acid dihydrate (SSA) were purchased from Millipore Sigma and Dinamica Quimica LTDA, respectively. Potassium dichromate ($K_2Cr_2O_7$, 99.5%) was acquired from Acros Organics. All chemicals were used without further purification.

2.2. Membrane fabrication

For electrospinning, PVDF-HFP polymer was dissolved sequentially in a binary mixture of DMF/acetone at a concentration of 20 wt%. To accomplish this, PVDF-HFP was first dissolved in DMF under vigorous stirring at 70 °C for 90 min. The solution was then cooled down to room temperature under stirring. A desired amount of acetone was subsequently added (the DMF/acetone ratio was kept at 60/40 v/v%) and stirred for another 30 min. The recovered PVDF-HFP homogeneous solution was electrospun at a voltage of 26 kV using the flow rate of 1.0 mL/h and with the tip-collector distance of 15 cm. The electrospinning instrument was set up vertically and the polymer solution was electrospun using a single capillary gauge needle (spinneret). The flow rate of the polymer solution was adjusted by a programmable KD Scientific syringe pump. The spinneret was connected to a Glassman high-voltage DC power supply and a grounded rotating drum collector, which was covered by a PET non-woven substrate (thickness around 190 μm). Uniform sheets of nanofibrous membranes with an average total membrane thickness (i.e., PET substrate and electrospun layer) of 220 (± 1.58) μm were obtained after 4 h of continuous electrospinning on a drum collector spinning at 50 rpm. During the electrospinning process, the temperature and relative humidity were maintained approximately at 24 °C and 40%, respectively. The nanofibrous membranes were then dried at room temperature.

To provide proper functional groups to the fibers for chromium removal, the as-prepared electrospun PVDF-HFP membrane was coated by *in-situ* polymerization of aniline, using the method described by Huang et al. [26]. Briefly, APS (0.02 mol) was first dissolved in 50 mL of deionized water to prepare solution I. Then, 0.02 mol of aniline was added into 50 mL of deionized water under stirring. After aniline was totally dissolved, 0.01 mol of 5-sulfosalicylic acid (SSA) was added to this solution and thoroughly mixed to generate solution II. Afterwards, solution I was added into solution II and stirred continuously to obtain a homogenous solution (i.e., the dipping solution). The PVDF-HFP membrane was then immersed in the dipping solution and was remained at room temperature for 5 h to generate a PAni coating layer on the surface of nanofibers through oxidative polymerization. Finally, the resulting membrane was taken out and washed three times with water and dried in an oven at 70 °C for 30 min.

2.3. Membrane characterization

A *CFP-1500A* capillary flow porometer *(Porous Materials Inc., USA)* was used to characterize the mean pore size, bubble point, wet/dry curves, and pore size distribution of the membranes. The Galwick fluid with a standard surface tension of 15.9 dynes was used to wet the membrane pores. The difference between the gas flow rates in the dry and wet states of the membrane as a function of applied pressure was translated into pore size using the Young-Laplace equation:

$$r = \frac{2\gamma}{\Delta P}.\cos\theta \quad (1)$$

where r is the pore radius; γ is the surface tension of the wetting fluid (Galwick); P is the gas pressure; and θ is the contact angle of the wetting fluid.

A Mitutoyo 547-500S micrometer was used to analyze the thickness of the membranes. The contact angle of the membranes was measured using the sessile drop method by a contact angle measuring device OCA15EC (DataPhysics, Germany). In this test, a 4 μL droplet of deionized water was dropped on the membrane and a computer-assisted camera was used to capture the image of the water droplet. The SCA20 software was used to analyze the image and calculate the contact angle value. The surface charge of the membranes was evaluated by Zetasizer Nano ZS ZEN3600 (Malvern Instruments) in fixed ionic strength at pH = 4.5 and room temperature. The porosity of the membrane was defined by the gravimetric method, using isopropyl alcohol as a wetting fluid to penetrate the pores of the membrane. Fourier transform infrared (FT-IR) spectra in the range of 1800–800 cm^{-1} were recorded using a Nicolet iS50 FT-IR Spectrometer with a built-in ATR mode to determine the functional groups of the membranes. The spectra were obtained at a resolution of 4 cm^{-1} and 64 scans per spectrum. The morphology of the electrospun nanofibrous scaffold was observed by a focused ion beam-scanning electron microscope (FIB-SEM, Zeiss model Crossbeam 340), operating at 30 kV. The samples were mounted on a carbon tape and sputter-coated in high vacuum with Au/Pd using a SC-7620 Mini Sputter Coater (Quorum Technology). The surfaces of the materials were analyzed using a PHI X-ray photoelectron spectrometer (XPS) with Al Kα1,2 (1486.6 eV) as X-ray source.

2.4. Adsorption tests

Potassium dichromate solutions with various Cr(VI) concentrations ranging from 10 to 600 mg/L were prepared to study the adsorption capacity of the membranes at different chromium concentration. In this test, a 10 mg of membrane sample was immersed in 15 mL of chromium solution at a chosen concentration and was shaken for 24 h. To analyze the pH effect, solutions with concentrations of 100 mg/L and pH values ranging from 1.5 to 7 were prepared. The contact time test was also carried out with a 100 mg/L Cr(VI) solution at a pH value of 4, where the sample was measured at a chosen time interval. For the regeneration study, the membrane was used to treat 15 mL of Cr(VI) solution (100 mg/L) for 2 h, and then the membrane was taken out and regenerated by immersing it into 15 mL of 0.5 M NaOH for 2 h, followed by protonation with 15 mL of 0.5 M HCl. For the dynamic adsorption test, a fixed volume (5 mL) of 50 mg/L Cr (VI) solution was first prepared, where the effect of the applied flux ranging from 0.5 to 5.0 mL/min was examined by injecting the solution through a dead-end filtration cell (Microsyringe Filter Holder -X3002500, Millipore). In addition, different volumes (1 to 35 mL) of Cr(VI) solutions at a fixed concentration of 5 mg/L were injected through the membrane at a constant flux of 0.5 mL/min.

The Cr(VI) concentration was determined by a UV–Visible spectrophotometer (Thermo Scientific, Genesys 10S) using the diphenylcarbazide solution as an indicator at 540 nm.[27] A calibration curve was created by plotting the absorbance versus known Cr(VI) concentrations for this test. The amount of Cr(VI) ions adsorbed on the membrane (mg/g) was calculated by the following equation:

$$Q = \frac{(C_O - C_f)V}{M} \tag{2}$$

where Q is the amount of Cr(VI) adsorbed (mg/g), C_O and C_f are the initial and final Cr(VI) concentrations (mg/L), respectively, V is the solution volume, and M is the weight of adsorbent membrane used. The Langmuir isotherm model was applied to determine the maximum adsorption capacity of the membrane.

$$\frac{C_e}{q_e} = \frac{C_e}{q_m} + \frac{1}{bq_m} \tag{3}$$

where q_e is the adsorption capacity of the membrane at the equilibrium concentration (mg/g), C_e is the equilibrium concentration of metal ion (mg/L), q_m is the maximum adsorption capacity of the membrane (mg/g), and b is the Langmuir constant.

3. Results and discussion

3.1. Membrane characterization

Fig. 1 shows the FT-IR spectra of pristine PVDF-HFP and PAni coated PVDF-HFP (denoted PVDF-HFP/PAni hereafter) membranes. Several sharp, high intensity peaks were observed in the PVDF-HFP membrane spectrum. The peak at 1400 cm^{-1} could be ascribed to the $-CH_2$ wagging vibrations [28]. The band at 1175 cm^{-1} was characteristic of the symmetrical stretching vibrations of $-CF_2$, where the small shoulder at around 1200 cm^{-1} was assigned to the asymmetric vibrations of this band [29,30]. The stretching vibrations of the $-CF_3$ was shown as the peak at 1073 cm^{-1} [29,31]. The peaks at 874 and 838 cm^{-1} corresponded to the absorptions of the C–F bands in the amorphous phase of the polymers [23,32]. With the coating of polyaniline, the characteristics peaks of the initial PVDF-HFP substrate were preserved but several new peaks appeared. The peaks at 1579 and 1494 cm^{-1} corresponded to the C=C stretching deformation in the quinoid and benzenoid rings, respectively [33–35]. The peak at 1302 cm^{-1} could be attributed to the C–N stretching vibration in the benzenoid ring [14,33]. The peaks centered at 1146 cm^{-1} was assigned to the aromatic C–H bending of the benzenoid ring and vibrations of the C–N–C group, indicating the electron delocalization of the quinoid rings [10,36].

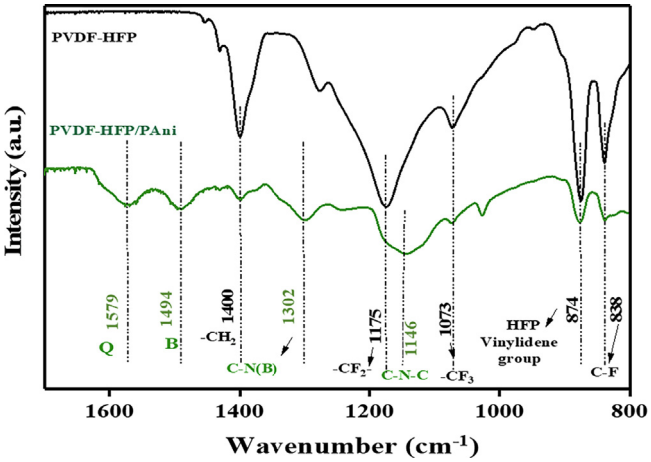

Fig. 1. FTIR spectra of the PVDF-HFP and PAni-coated membranes.

The pore size and pore size distribution of the pristine and PAni-coated PVDF-HFP nanofibrous membranes were evaluated using the gas permeability of the dry sample (dry curve) followed by that of the wetted sample (wet curve). As shown in Fig. 2(a), the pristine PVDF-HFP membrane allowed more gas to permeate in the same pressure

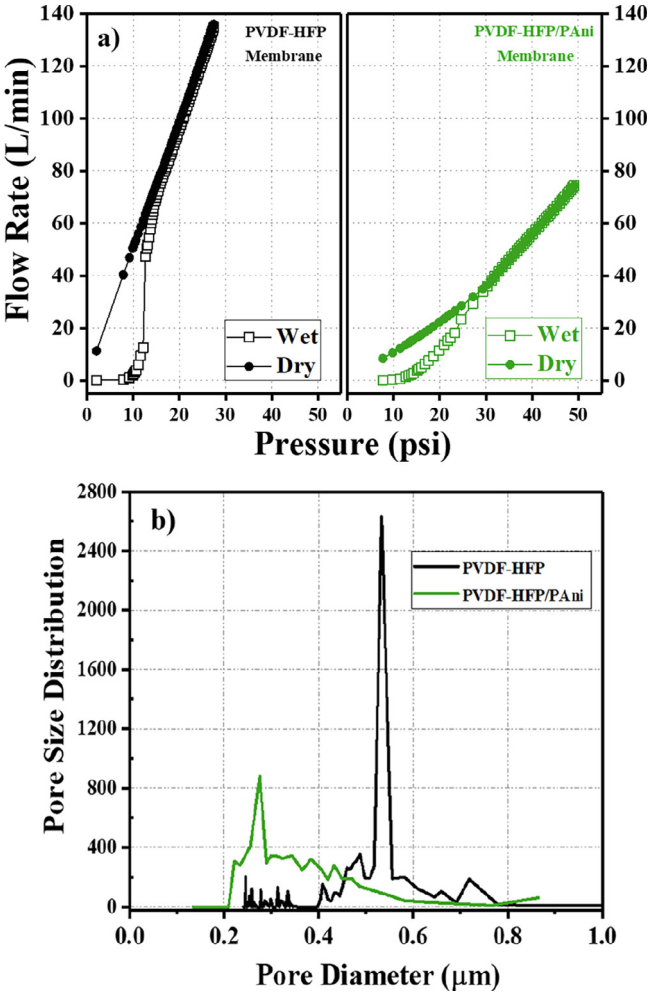

Fig. 2. (a) Dry-wet curves and (b) pore size distribution of the membranes before and after polyaniline coating.

range when compared with the PVDF-HFP/PAni membrane. In addition, all wetting fluid passed through the pores of the pristine PVDF-HFP membrane at 14 psi, while in the polyaniline-coated membrane, the applied pressure was 26 psi. This indicates that the pristine membrane possessed larger pore sizes and it took lower gas pressures to completely push the wetting liquid through the membrane. However, when polyaniline was deposited on the nanofiber surface, the effective pores became smaller, where higher pressure was required. This clearly showed that the *in-situ* polymerization of aniline on the PVDF-HFP nanofibrous scaffold reduced the pore volumes. This phenomenon was also manifested by the reduction of the bubble point for the membrane after the coating (~1.6 μm for PVDF-HFP *vs.* ~0.9 μm for PVDF-HFP/PAni). In addition, the drying process of the wetted PVDF-HFP membrane occurred at a very narrow pressure range (10–14 psi), while the drying of the wetted PVDF-HFP/PAni membrane started at 10 psi and continued up to 26 psi. This demonstrates that the pristine membrane possessed a very narrow pore size distribution, whereas the polyaniline-coated membrane possessed a wide range of pore sizes. Fig. 2(b) exhibits the pore size distribution of the two membranes. As discussed earlier, the PVDF-HFP membrane showed a uniform pore size distribution at ~0.5 μm, while PVDF-HFP/PAni exhibited a broader pore size distribution with a peak at ~0.3 μm.

Fig. 3 illustrates the contact angles of the PVDF-HFP and PVDF-HFP/PAni membranes. The pristine PVDF-HFP membrane exhibited a very high contact angle due to the intrinsic low surface energy of the fluorine in fluoropolymer. This low surface energy was further exacerbated by the electrostatic charge introduced by the electrospinning process, where it favored the fabrication of more hydrophobic membrane surfaces. Diffusion of the contaminated water into the adsorbent membrane is a main issue for the removal of contaminants via adsorption. Electrospun PVDF-HFP membrane with a contact angle of ~132° had a weak affinity towards water molecules and thus, the water media could not penetrate into the adsorbent membrane pores [14,37–40]. However, the PAni coating drastically reduced the water contact angle of the membrane to ~45°, suggesting that the surface of electrospun PVDF-HFP nanofibers were completely coated with more hydrophilic polyaniline polymers [41]. The decrease in water contact angle could be attributed to the introduction of the imine moieties of PAni anchored to the nanofibers, which significantly increased the affinity of the PVDF-HFP/PAni membrane. In addition, since the imine groups are prone for protonation and provide ammonium ions, the increase in the hydrophilic properties of the membrane greatly improved the transfer of Cr(VI) ions into the fibrous scaffold [18].

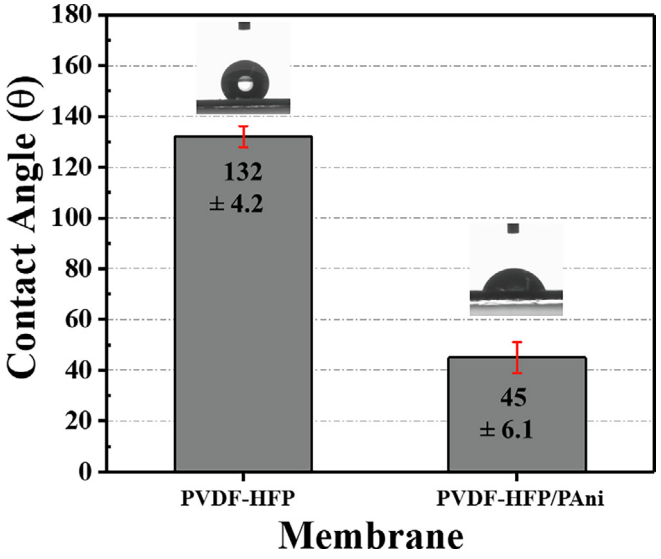

Fig. 3. Water contact angle of PVDF-HFP and PVDF-HFP/PAni membranes.

The SEM micrographs of nanofibrous scaffolds before and after the PAni coating are illustrated in Fig. 4. It was seen that the pristine PVDF-HFP membrane had much larger surface pores compared with the PVDF-HFP/PAni membrane. This confirmed the pore size distribution results obtained earlier by the porometer. Furthermore, the histograms of the fiber diameter for the two membranes (Fig. 4c and d) indicate that the fiber diameters increased in the PVDF-HFP/PAni membrane (the average fiber diameter increased from 127 to 141 nm after the polyaniline coating). This is very reasonable as during *in-situ* polymerization, the aniline monomers are first absorbed on the PVDF-HFP nanofibers and then polymerized, making a polymeric layer on the nanofiber surface. This was also consistent with the slight increase in the scaffold thickness (Table 1).

3.2. Adsorption performance

3.2.1. Static adsorption

The adsorption test of the pristine PVDF-HFP membrane against Cr (VI) indicated that the unmodified membrane was non-effective. As a result, only the adsorption performance of the PVDF-HFP/PAni membrane is reported here. Fig. 5(a) shows the adsorption capacity of PVDF-HFP/PAni against Cr(VI) at different concentrations. According to the adsorption isotherm, the equilibrium adsorption capacity of the membrane exhibited a sharp increase by increasing the chromium concentration and then, reached a plateau value. This indicates that any further increase in the chromium concentration would not significantly affect the chromium uptake of the membrane. The presence of the imine groups in polyaniline was responsible for the removal of oxy anionic species due to the presence of electron donors of PAni in emeraldine form. The mechanism of negatively-charged dichromate uptake by the PAni-coated membrane is believed to occur in two stages: 1) initially, the dichromate oxyanion was hydrolyzed and existed in the predominant form of $HCrO_4^-$ in the pH range of 2 to 6, which could, in turn, interact electrostatically with the positively-charged imine groups of the PAni-coated membrane:

$$Cr_2O_7^{2-} + H_2O \leftrightarrow 2HCrO_4^- \quad (4)$$

2) Due to the presence of electron donors of PAni, Cr(VI) was subsequently reduced to Cr(III) according the following reaction, while the emeraldine salt of the polymer was simultaneously oxidized into pernigraniline form:

$$HCrO_4^- + 7H^+ + 3e^- \leftrightarrow Cr^{3+} + 4H_2O \quad (5)$$

Generally, electrostatic interaction between the negatively-charged dichromate and positively-charged polyaniline followed by a redox reaction was the major mechanism for the simultaneous adsorption and reduction of Cr(VI). The adsorption and oxidation-reduction mechanisms have been schematically illustrated in Fig. 5(b) [22,36,42–44]. Polyaniline was previously evaluated as a good adsorbent for the removal of heavy metal ions from water, and has been used in a composite format, such as nanocomposites of MoS_2/PAni immobilized in PAN nanofibers [12]. PAni/MnO_2/TiO_2 nanocomposites [16], ethyl cellulose coated by PAni [20], folic-acid-polyaniline hybrid hydrogel [17], jute fibers coated by PAni [20] and polyacrylonitrile/polyaniline core/shell nanofibers [45].

The Cr(VI) adsorption isotherm of the membrane was analyzed using the Langmuir adsorption isotherm model. It was found that the analysis showed a good linear relationship between C_e/Q_e and C_e with a high coefficient of determination (R^2 = 0.986). The Freundlich and the Redlich-Peterson models were also evaluated in the linearized form with the R^2 values of 0.888 and 0.970, respectively (Figs. S1 and S2). The better fit of the Langmuir adsorption isotherm model confirmed a monolayer adsorption process, implying that the Cr(VI) adsorption was occurring at a limited number of localized sites of the imine groups in the PAni structure. In other words, there were little or no lateral interactions and steric hindrance between the adsorbates [42]. The

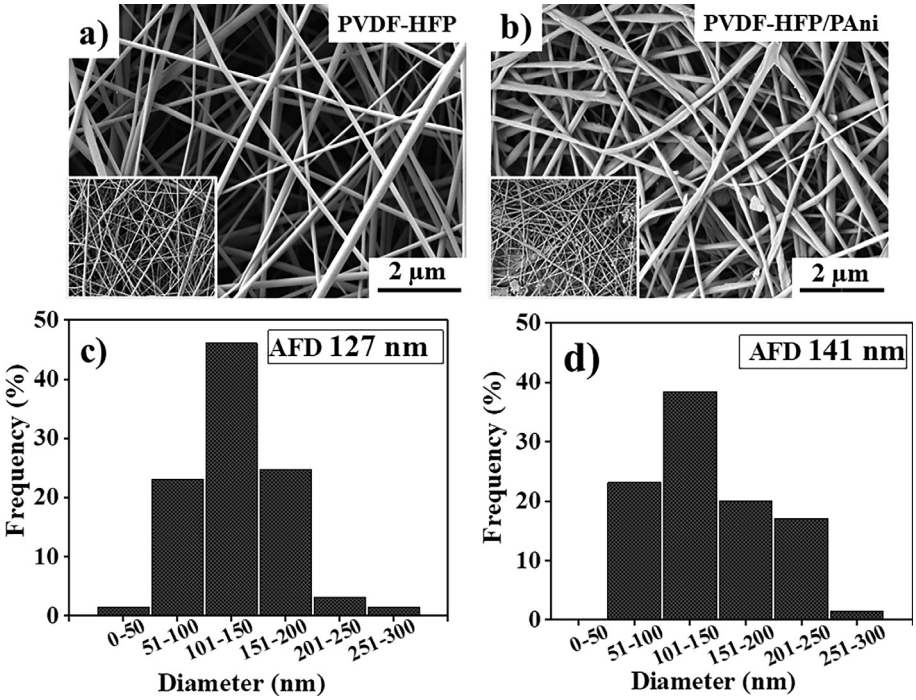

Fig. 4. SEM images of (a) PVDF-HFP membrane and (b) PVDF-HFP/PAni membrane. Histograms showing fiber diameter distribution for (c) PVDF-HFP membrane; and (d) PVDF-HFP/PAni membrane.

Table 1
Characteristics of the as-prepared and PAni-coated membranes.

	Thickness (µm)	Contact Angle (°)	Average Fiber Diameter (nm)	Bubble Point Size (µm)	Mean Pore Size (µm)	Porosity (%)
PVDF-HFP	220.3 ± 1.6	132 ± 4	127.0	1.57 ± 0.75	0.54 ± 0.07	86.82 ± 0.01
PVDF-HFP/PAni	232.2 ± 4.2	45 ± 6	140.7	0.87 ± 0.91	0.34 ± 0.46	75.89 ± 0.02

maximum adsorption capacity (q_m) of the PVDF-HFP/PAni membrane for Cr(VI) was calculated to be around 15.08 mg/g (pH 4.5), determined by the Langmuir isotherm model. Li et al. found that the maximum static adsorption capacity of chitosan nanofibers electrospun on polyester polyester for Cr(VI) was ~11.0 mg/g [46]. PAni nanocomposites with fiber glass and poly(ethylene terephthalate) (PET) showed capacities as low as 3.2 mg/g for dichromate [47]. Karthik et al. prepared a PAni-silica gel composite and achieved an adsorption capacity of 23.0 mg/g [13]. Espinoza demonstrated that the adsorption capacity of PAni-electrospun PS composite could be enhanced using plasma treatment [14]. The plasma-treated PAni-PS composite showed a chromium adsorption capacity of 58 mg/g. However, plasma treatment is a costly technique and does not seem to be practical in real applications. A summary of the adsorption capacities of the PAni-related materials have been given in Table S1.

The dimensionless separation factor, R_L, is a critical parameter to evaluate the favorability of an adsorption process [13,48]. R_L can be defined by the following equation:

$$R_L = \frac{1}{1 + bC_O} \tag{6}$$

where b is the Langmuir isotherm constant and $C_O$is the initial concentration of the adsorbate (in this case, Cr(VI)). When$R_L = 0$, the adsorption is strong and it can be considered as irreversible; $R_L = 1$ indicates a linear adsorption; when $0 < 1 < R_L$, the adsorption is considered favorable and reversible; $R_L > 1$ suggests an unfavorable adsorption that can only occur in the binary mixtures. The separation factor (R_L) of the Cr(VI) by the PVDF-HFP/PAni membrane was found to be around 0.005, which indicated that the sorption process was highly favorable.

The effect of contact time on the Cr(VI) removal is shown in Fig. 6(a). The Cr(VI) removal efficiency was found to increase steadily over the time period of 24 h and then subsequently reached a plateau value, where no more adsorption occurred. It was found that the Cr(VI) adsorption amount increased to 7.60 mg/g in the first 10 h and reached a plateau value of 12.12 mg/g after 24 h.

Two models, pseudo first-order and pseudo second-order models, were used to analyze the nature of the kinetics and the rate of Cr(VI) adsorption by the PVDF-HFP/PAni membrane. The linear forms of these two models are given in Eqs. (5) and (6), respectively.

$$\log(q_e - q_t) = \log q_e - \frac{k_1}{2.303}t \tag{7}$$

$$\frac{t}{q_t} = \frac{1}{q_e}t + \frac{1}{k_2 q_e^2} \tag{8}$$

where q_e and q_t denote the amount of Cr(VI) adsorbed on the membrane at equilibrium and at time t, respectively, k_1 and k_2 are the first and second-order rate constants, respectively. According to Fig. 6(c), the adsorption followed a pseudo first-order reaction, manifested by a higher correlation coefficient value (R^2) obtained by the linear form of this model. This indicates that the adsorption process of Cr(VI) may be considered a physisorption process at least at the later stages of the adsorption. However, these results should be interpreted with some caution, as in major cases, there is a combination of physisorption and chemisorption. Also, the intensity and rate of these two phenomena may drastically change by time. Therefore, although the pseudo first-order model suggests a physisorption, we are not inclined to conclusively and strictly exclude the possible occurrence of the chemisorption mechanism.

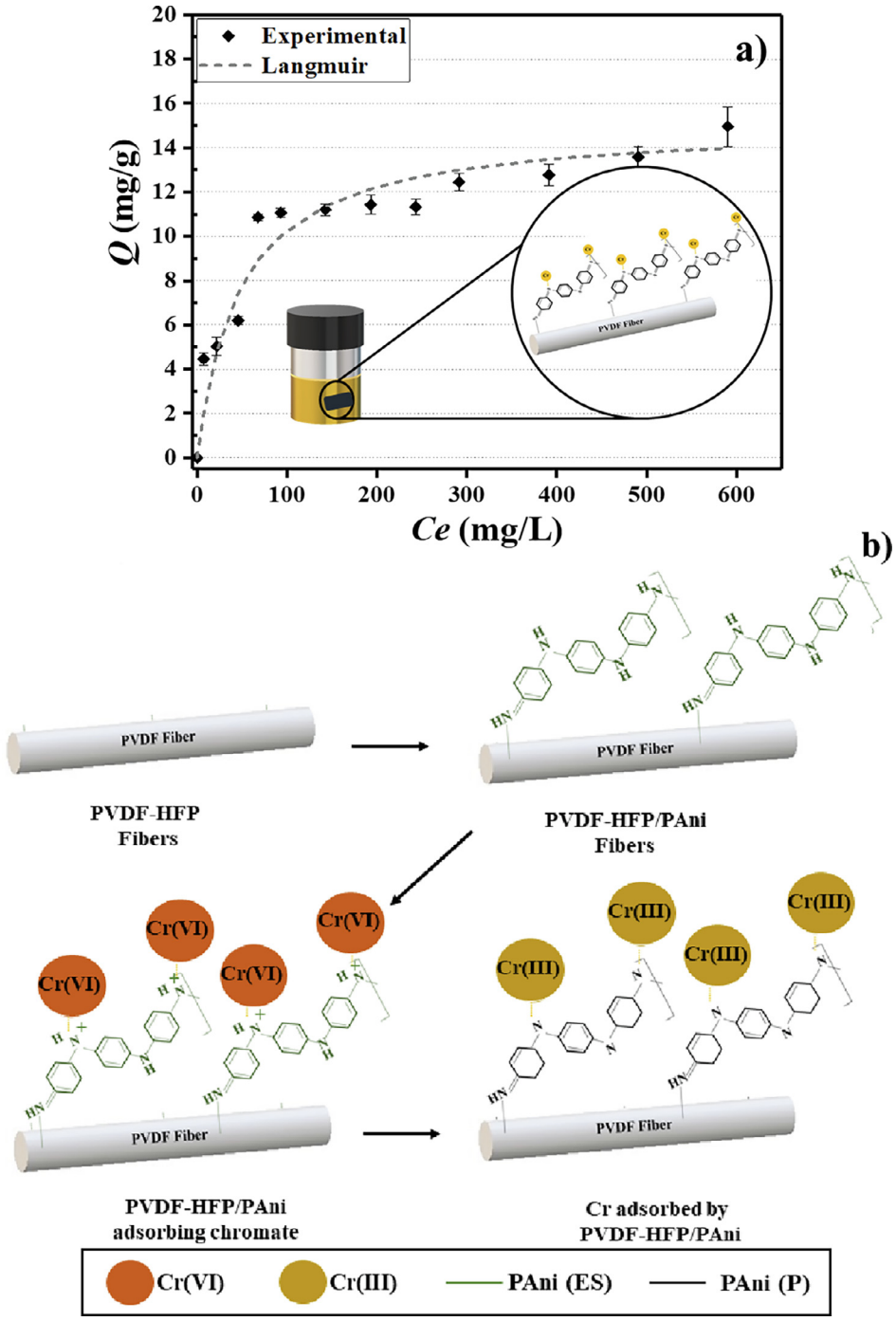

Fig. 5. (a) The chromium adsorption isotherm of the PVDF-HFP/PAni adsorbent membrane. (b) Simultaneous adsorption and oxidation-reduction mechanisms. (c) Linearized chromium adsorption isotherm by the Langmuir model.

The effect of pH on the adsorption capacity of Cr(VI) is shown in Fig. 7. It was found that the adsorption capacity exhibited a decreasing trend with increasing pH value. The highest Cr(VI) adsorption capacity (~40.50 mg/g) was found in the lowest pH value and a sharp decrease in the adsorption capacity (~23.60 mg/g) was observed when the pH value increased to ~2. The notable pH dependence of the Cr(VI) adsorption capacity on the PVDF-HFP/PAni membrane could be related to both the predominance of various chromium species (chromium speciation) at different pH values or the change in the reduction rate of Cr (VI) by pH level. At pH values lower than 2, most of the chromium is in chromic acid (H_2CrO_4) form [49]. When the pH value is between 2 and 6, the predominant species is hydrogen chromate ($HCrO_4^-$) coexisting with dichromate ions ($Cr_2O_7^{2-}$). Ultimately, at the pH values above 6, the dominant species is chromate (CrO_4^{2-}) [3,10,13,50]. On the other hand, in an acidic media, the adsorbent (in this case, the PVDF-HFP/PAni membrane) was also protonated and formed a positively-charged surface with NH^+ functional groups. Therefore, at very low pH values, the highly protonated membrane surface favored the adsorption of the chromium species as a result of the electrostatic attraction between the iminium ions and the oxyanions. As the pH value increased, the protonation of the membrane surface was relatively declined, which induced lower electrostatic attraction with the free oxyanion, reflected as lower adsorption capacity [2,51]. The decrease in the reduction rate of Cr(VI) by increasing the pH could also explain this trend.

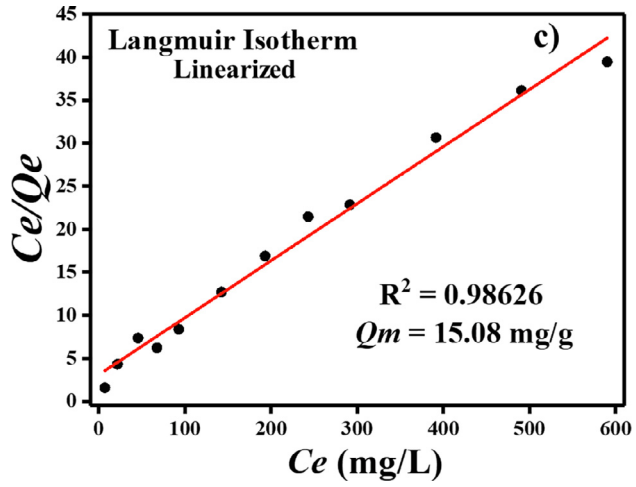

Fig. 5. (*continued*)

in an acidic environment. The adsorption-desorption process was repeated for 5 cycles, where the results indicated that the PVDF-HFP/PAni membrane still exhibited good desorption capacity above 70% even after 5 cycles. This indicates that the PVDF-HFP/PAni membrane possessed a high number of adsorption sites and the recoverability of the occupied adsorption sites was effective.

3.2.2. Dynamic adsorption

The dynamic chromium adsorption for the PVDF-HFP/PAni membrane obtained at different flow rates of the feed solution are presented in Fig. 9(a). At the low flow rate (e.g., 0.5 mL/min), the membrane exhibited the highest chromium uptake, which could be explained by the higher contact time of Cr(VI) ions with the active sites of the PAni surface. When the flow rate increased to 1.0 mL/min, the chromium uptake was found to decline, however, further increase in the flow rate did not impact the adsorption capacity. Fig. 9(b) illustrates the chromium uptake of the PVDF-HFP/PAni membrane at a fixed flow rate of 0.5 mL/min as a function of the Cr-laden water volume passing through

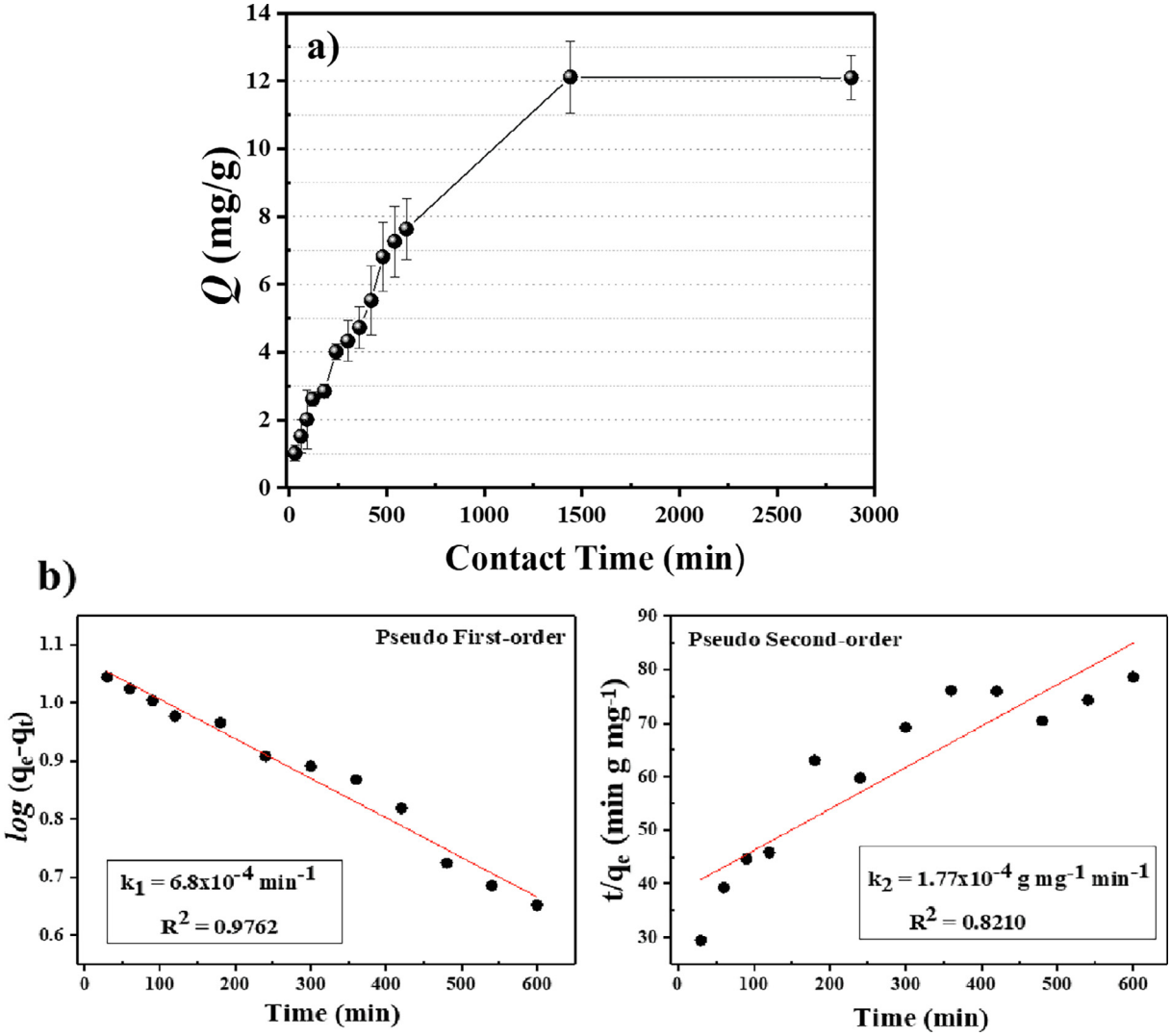

Fig. 6. (a) The effect of the contact time on the adsorption of Cr(VI) (C_0 = 100 ppm); (b) The adsorption kinetic modeling using a pseudo first-order and pseudo second-order models.

The efficient regeneration of the used PVDF-HFP/PAni membranes was carried out by a facile two-step chemical treatment method, as illustrated in Fig. 8. In this treatment, the chromium was desorbed in an alkaline environment, followed by the protonation of the PAni surface the membrane. The membrane uptake capacity was found to increase when a higher volume of contaminated water passed through the membrane, and the capacity finally reached a plateau value. Evidently, as the chromium concentration increased, the membrane uptake

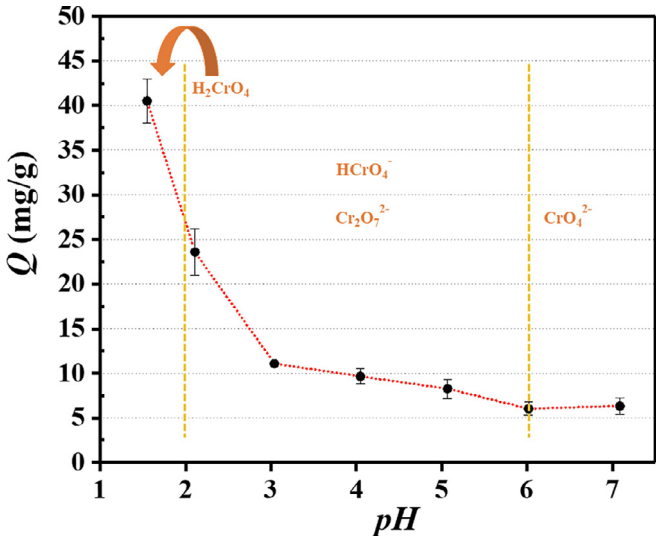

Fig. 7. The effect of pH on the Cr(VI) adsorption capacity of the PVDF-HFP/PAni membrane.

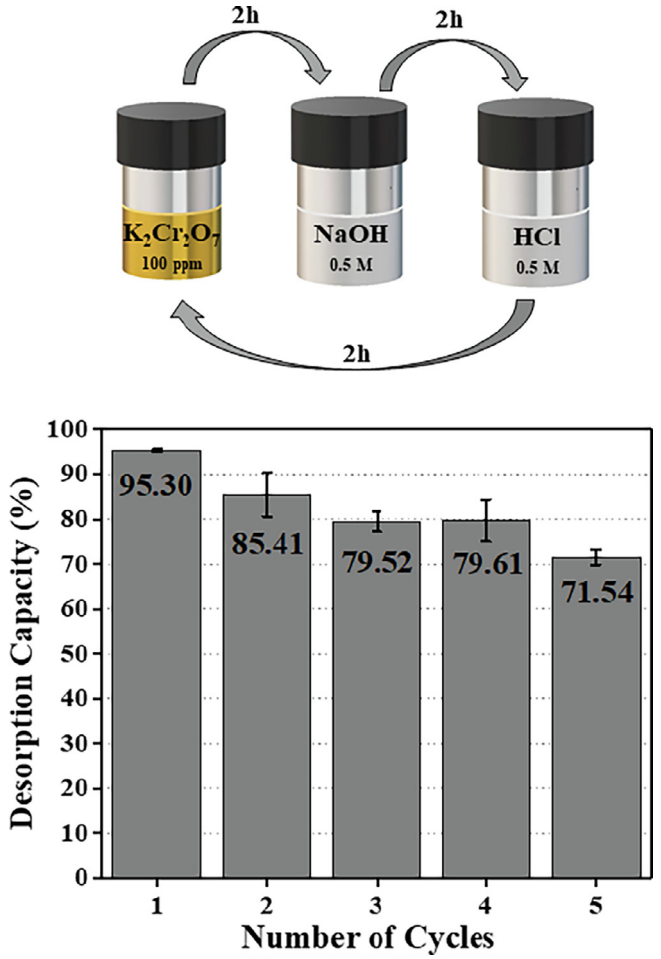

Fig. 8. The regeneration/recyclability efficiency of the PVDF-HFP/PAni membrane.

capacity also increased.

3.2.3. Characterization of the used membrane

The mapping of the chromium on the adsorbed membrane obtained by energy dispersive X-ray (EDX) is illustrated in Fig. 10. This figure

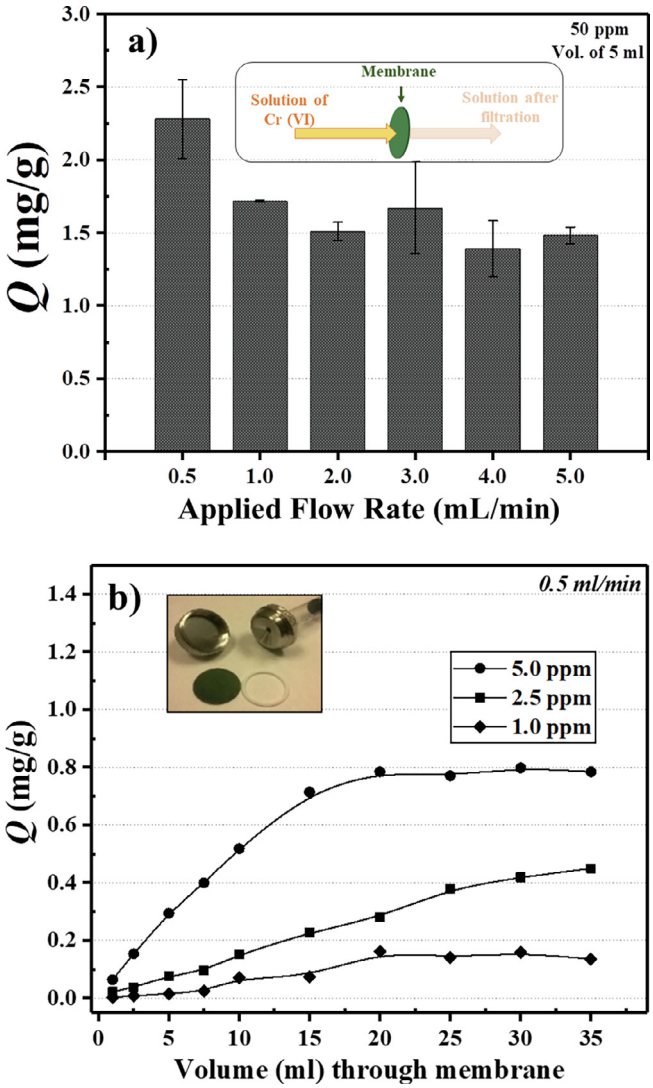

Fig. 9. (a) Effect of the applied flow rate, and (b) the injected volume through the on the adsorption capacity of the PVDF-HFP/PAni membrane.

depicts that a large amount of chromium was uniformly distributed throughout the fibers present on the nanofibrous scaffold surface after the adsorption process. The uniform distribution of the chromium on the nanofibers also indicated that the polymerization homogeneously occurred throughout the fiber surface, and thus the adsorption functional groups (imide and amine) were well-distributed in the substrate. A significant change in the morphologies of the membranes before and after the chromium adsorption can be detected. Partial oxidation of emeraldine to pernigraniline can lead to lower PAni crystallinity [52], change the configuration of the polymeric chains, and lead to notable morphological changes. However, this morphological change did not affect the integrity of the adsorptive membrane, as the membranes could be used in several regeneration-reuse cycles.

The valence states of chromium and the types of the functional moieties in the chromium-adsorbed PVDF-HFP/PAni was determined by XPS, where the results are shown in Fig. 11. It was found that the presence of F1s and N1s peaks in the wide scan spectrum was indicative the PVDF-HFP nanofibers and PAni characteristics, respectively. In addition, the Cr2p peak evidently confirmed the adsorption of the chromium species on the membrane. The Auger peaks of chromium in Fig. 11(c) presented an insight into the oxidation state of adsorbed chromium. In specific, two Auger peaks at binding energies of 592.8 and 583.1 eV represented Cr(III), confirming that the hexavalent

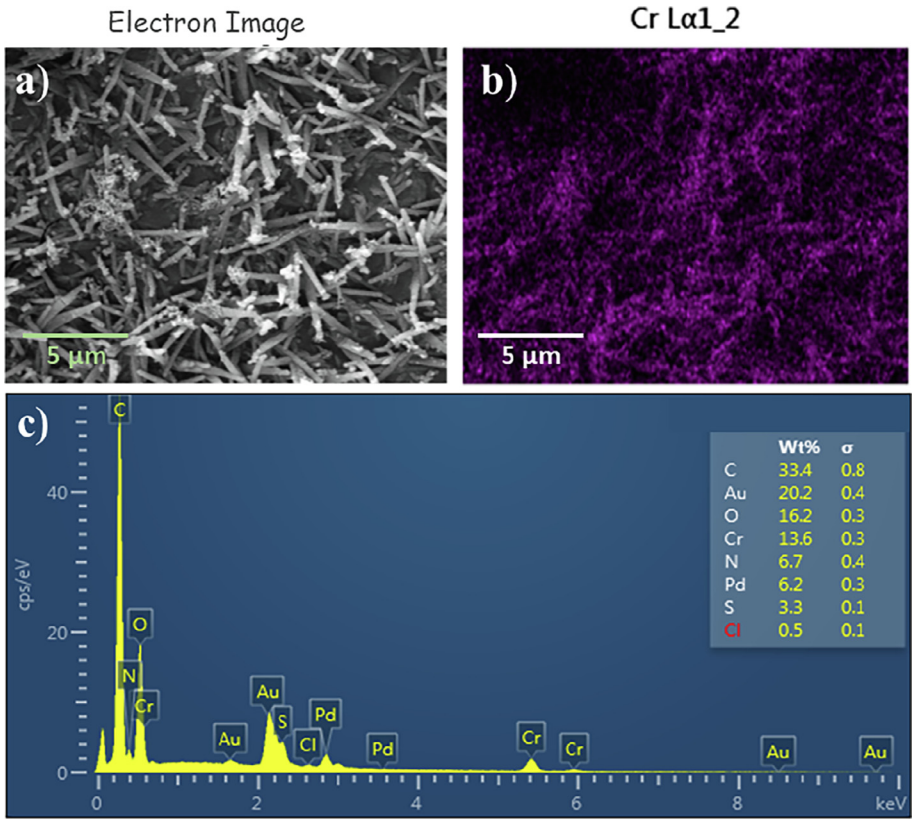

Fig. 10. a) SEM image, b) chromium mapping, and c) EDX spectrum of the PVDF-HFP/PAni after adsorption.

chromium was reduced to trivalent chromium during the adsorption, corroborating the adsorption mechanism explained previously. The deconvolution of the N1s spectrum yielded four distinguishable nitrogen components: binding energies at 396.3 eV could be attributed to N atoms that are sp2-bonded to two carbon atoms in the quinoid imine units (−N═), 398.6 eV corresponded to the tertiary nitrogen bonded in the benzenoid units (−NH), and 400.5 and 404.6 eV from the amine peak commonly attributed to the protonated species (N+) which can be ascribed to the chelation of Cr(III) during the redox reactions between the adsorbate and adsorbent. Moreover, this last peak can be assigned to the doping process of H+ on the quinoid amine. This analysis indicated that nitrogen is found as both protonated and unprotonated states on the membrane surface [53–57]. Ding et al. carried out similar XPS experiments on the polymer-PAni adsorptive membranes before and after adsorption. They observed that the intensity of the peak assigned to N+ either decreased or disappeared depending on the adsorption capacity [58]. They indicated this phenomenon to the electrostatic interaction between the PAni and the Cr(VI)

Fig. 12 illustrates the zeta potential values of the PVDF-HFP nanofibrous membrane before and after the PAni deposition via in situ polymerization and the PVDF-HFP/PAni membrane after chromium adsorption (PVDF-HFP/PAni_Cr). It was observed that the pristine electrospun PVDF-HFP exhibited a partially negatively charged surface with a zeta potential value of −14.9 ± 3.7 mV. PAni-coating rendered the surface of the membrane positively-charged (+37.7 ± 4.3) by introducing positively-charged imine groups of the emeraldine salt. This is consistent with the XPS measurements and proves the presence of emeraldine salt on the electrospun fibers. After the adsorption, the zeta potential of the membrane decreases to −18.5 ± 4.6 which is very close to the pristine PVDF-HFP membrane. This reflects that the imine groups on the PVDF-HFP/PAni were reduced to uncharged form upon the adsorption of dichromate, consistent with the proposed simultaneous adsorption and oxidation-reduction mechanism.

4. Conclusions

The PVDF-HFP/PAni membrane was successfully prepared by electrospinning of a nanofibrous scaffold followed by *in-situ* polymerization of a uniform polyaniline coating on the nanofibers. The morphology, pores size and water contact angle of the resulting membranes with and without PAni coating were carefully evaluated. From the chromium removal test, it was found that the maximum adsorption capacity of the PVDF-HFP/PAni membrane was 15.08 mg/g (at pH = 4.5), where both pH and time were found to affect the adsorption efficiency. From dynamic adsorption test, the best performed flux was about 0.5 mL/min. When 20 mL of chromium solution passed though the membrane, a stable plateau adsorption capacity was observed. The EDX and XPS results confirmed the presence of Cr in the adsorbed membrane. This study suggested that the PAni coating can be very effective to apply to many other electrospun nanofibrous scaffolds to make adsorptive membranes in filtration systems.

Acknowledgements

This work was supported by FAPESP-Brazil (Sao Paulo Research Foundation) [grant number 2015/21261-2 and 2017/03638-7]. The authors also would like to thank the Center for Clean Water Technology from the New York State Department of Environmental Conservation; the National Science Foundation [DMR-1808690]; and the National Natural Science Foundation of China [51673011].

Appendix A. Supplementary data

Supplementary data to this article can be found online at https://doi.org/10.1016/j.cej.2019.04.154.

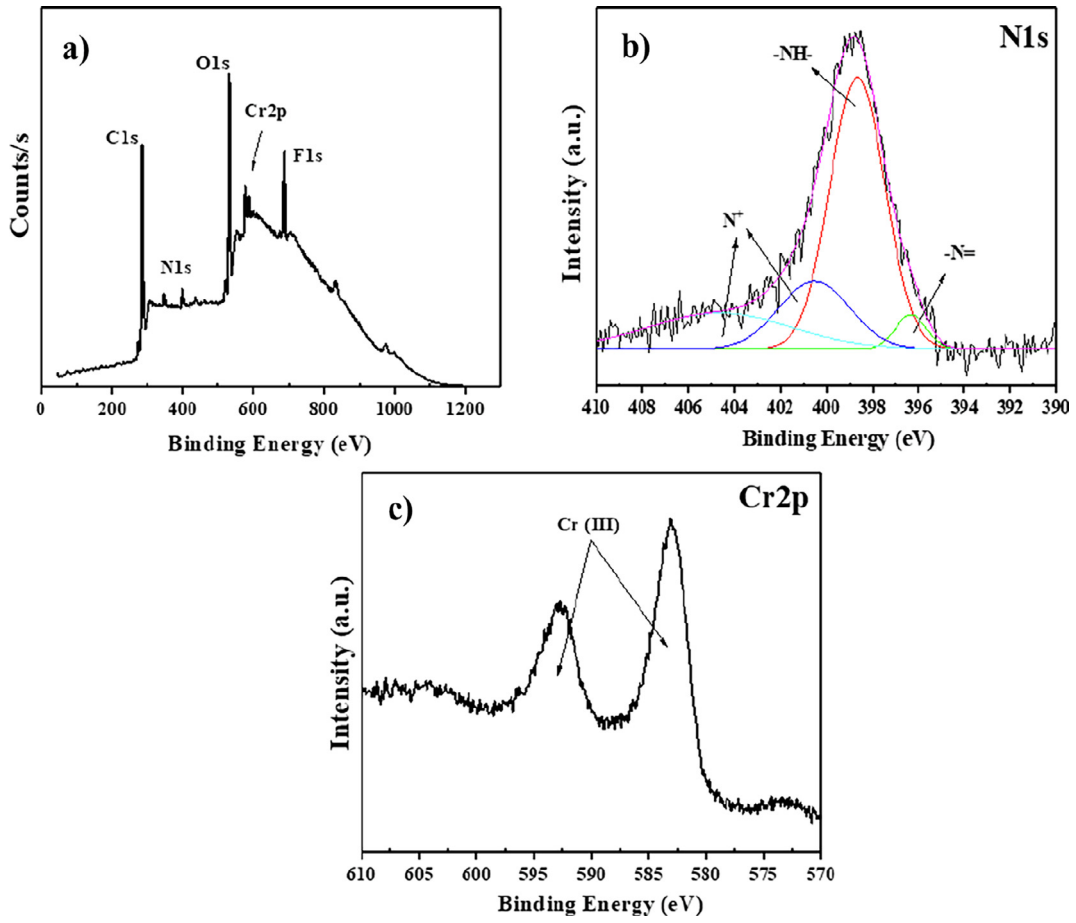

Fig. 11. The XPS analysis of the PVDF-HFP/PAni after the chromium adsorption: (a) XPS wide scan, (b) spectrum of N1s, and (c) spectrum of Cr2p.

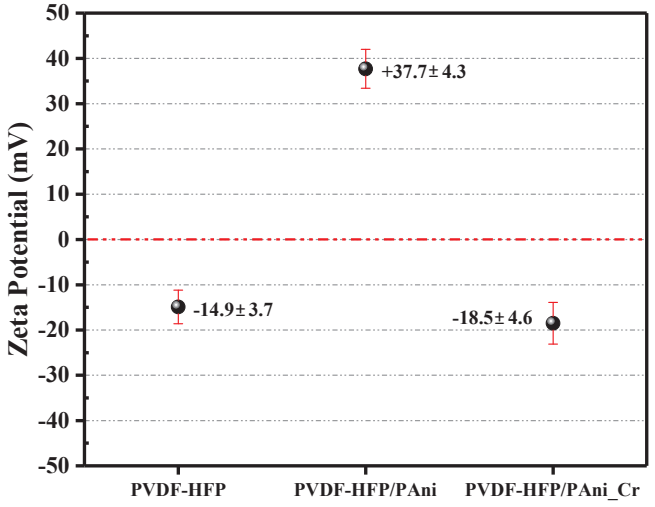

Fig. 12. Zeta potential values of the PVDF-HFP, PVDF-HFP/PAni and PVDF-HFP/PAni_Cr membranes at pH = 4.5.

References

[1] G. Ozdemir, N. Ceyhan, T. Ozturk, F. Akirmak, T. Cosar, Biosorption of chromium (VI), cadmium(II) and copper(II) by *Pantoea sp*. TEM18, Chem. Eng. J. 102 (3) (2014) 249–253.

[2] X. Guo, G.T. Fei, H. Su, L.D. Zhang, High-performance and reproducible polyaniline nanowire/tubes for removal of Cr(VI) in aqueous solution, J. Phys. Chem. C 115 (2011) 1608–1613.

[3] Y. Liu, H. Ma, B. Liu, B.S. Hsiao, B. Chu, B. High-performance nanofibrous membrane for removal of Cr(VI) from contaminated water, J. Plastic Film Sheeting 31 (4) (2015) 379–400.

[4] A.B. Albadarin, C. Mangwandi, A.H. Al-Muhtaseb, G.M. Walker, S.J. Allen, M.N.M. Ahmad, Kinetic and thermodynamics of chromium ions adsorption onto low cost dolomite adsorbent, Chem. Eng. J. 179 (2012) 193–2002.

[5] WHO, Guidelines for Drinking Water Quality, third ed. (2006).

[6] H. Demiral, I. Demiral, F. Tumsek, B. Karabacakoglu, Adsorption of chromium (VI) from aqueous solution by activated carbon derived from olive bagasse and applicability of different adsorption models, Chem. Eng. J. 144 (2008) 188–196.

[7] C. Pan, L.D. Troyer, P. Liao, J.G. Catalano, W. Li, D.E. Giammar, Effect of humic acid on the removal of chromium (VI) and the production of solids in iron electrocoagulation, Environ. Sci. Technol. 51 (2017) 6308–6318.

[8] M.K. Kim, K.S. Sundaram, G.A. Iyengar, K.P. Lee, A novel chitosan functional gel included with multiwall carbon nanotube and substituted polyaniline as adsorbent for efficient removal of chromium ion, Chem. Eng. J. 267 (2015) 51–64.

[9] C.J. Lin, S.L. Wang, P.M. Huang, Y.M. Tzou, J.C. Liu, C.C. Chen, J.H. Chen, C. Lin, Chromate reduction by zero-valent Al metal as catalyzed by polyoxometalate, Water Res. 43 (2009) 5015–5022.

[10] J. Ren, X. Huang, N. Wang, K. Lu, X. Zhang, W. Li, D. Liu, Preparation of polyaniline-coated polyacrylonitrile fiber mats and their application to Cr(VI) removal, Synth. Metals 222 (2016) 255–266.

[11] Z.J. Lin, H.Q. Zheng, H.Y. Zheng, L.P. Lin, Q. Xin, R. Cao, Efficient capture and effective sensing of $Cr_2O_7^{2-}$ from water using a zirconium metal-organic framework, Inorg. Chem. 56 (2017) 14178–14186.

[12] J. Qiu, F. Liu, S. Cheng, L. Zong, C. Zhu, C. Ling, A. Li, Recyclable nanocomposite of flowerlike MoS_2@Hybrid acid-dopes PAni immobilized on porous PAN nanofibers for the efficient removal of Cr(VI), ACS Sustain. Chem. Eng. 6 (2018) 447–456.

[13] R. Karthik, S. Meenakshj, Removal of hexavalent chromium ions using polyaniline/silica gel composite, J. Water Proc. Eng. 1 (2014) 37–45.

[14] J.J. Alcaraz-Espinoza, A.E. Chaves-Guajardo, J.C. Medina-Llamas, C.A.S. Andrade, C.P. Melo, Hierarchical composite polyaniline-(electrospun polystyrene) fibers applied to heavy metal remediation, Appl. Mater. Interfaces 7 (2015) 7231–7240.

[15] D. Li, J. Huang, R.B. Kaner, Polyaniline nanofibers: a unique polymer nanostructure for versatile applications, Acc. Chem. Res. 42 (2008) 135–145.

[16] B. Vellaichamy, P. Periakaruppan, B. Nagulan, Reduction of Cr^{6+} from wastewater using a novel in situ-synthesized PAni/MnO_2/TiO_2 nanocomposite: renewable, selective, stable, and synergistic catalysis, ACS Sustain. Chem. Eng. 5 (2017) 9313–9324.

[17] S. Das, P. Chakraborty, R. Ghosh, S. Paul, S. Mondal, A. Panja, A.K. Nandi, Folic acid-polyaniline hybrid hydrogel for adsorption/reduction of chromium(VI) and

selective adsorption of anionic dye from water, ACS Sustain. Chem. Eng. 5 (2017) 9325–9337.
[18] B. Qiu, C. Xu, D. Sun, H. Yi, J. Guo, X. Zhang, H. Qu, M. Guerrero, X. Wang, N. Noel, Z. Luo, Z. Guo, S. Wei, Polyaniline coated ethyl cellulose with improved hexavalent chromium removal, ACS Sustain. Chem. Eng. 2 (2014) 2070–2280.
[19] E.M. Al-Kinani, Studies on removal of hexavalent chromium ion from aqueous solution using polyaniline composite, J. Al-Nahrain Univ. 19 (2) (2016) 58–68.
[20] P.A. Kumar, S. Chakraborty, M. Ray, Removal and recovery of chromium from wastewater using short chain polyaniline synthesized on jute fiber, Chem. Eng. J. 141 (2008) 130–140.
[21] A. Olad, R. Nabavi, Application of polyaniline for the reduction of toxic Cr(VI) in water, J. Hazard. Mater. 147 (2007) 845–851.
[22] B. Qiu, C. Xu, D. Sun, Q. Wang, H. Gu, X. Zhang, B.L. Weeks, J. Hopper, T.C. Ho, Z. Guo, S. Wei, Polyaniline coating with various substrates for hexavalent chromium removal, Appl. Surf. Sci. 334 (2015) 7–14.
[23] R.A. Senthil, J. Theerthagiri, J. Madhavan, A.K.M. Arof, High performance dye-sensitized solar cell based on 2-mercaptobenzimidazole doped poly(vinylidine-fluoride-co-hexafluoropropylene) based polymer electrolyte, J. Macromol. Sci. Pure Appl. Chem. 53 (4) (2016) 245–251.
[24] M.M. Noor, M.H. Buraidah, M.A. Careem, S.R. Majid, A.K.M. Arof, An optimized poly(vinylidene fluoride-hexafluoropropylene)- NaI gel polymer electrolyte and its application in natural dye sensitized solar cells, Electrochem. Acta 121 (2014) 159–167.
[25] J.H. Cao, B.K. Zhu, G.L. Ji, Y.Y. Xu, Preparation and characterization of PVDF–HFP microporous flat membranes by supercritical CO_2 induced phase separation, J. Membr. Sci. 266 (2015) 102–109.
[26] R. Huang, Y. Long, C. Tang, H. Zhang, Fabrication of nano-branched coaxial polyaniline/PVDF-HFP fibers via electrospinning for strain sensor, Adv. Mater. Res. 853 (2014) 79–82.
[27] L.S. Clesceri, A.E. Greenberg, A.D. Eaton, Standard Methods for the Examination of Water and Wastewater, 20th ed., 1998, Maryland, USA.
[28] H. Bai, X. Wang, Y. Zhou, L. Zhang, Preparation and characterization of poly(vinylidene fluoride) composite membranes blended with nano-crystalline cellulose, Prog. Natl. Sci. 22 (3) (2012) 250–257.
[29] Y. Zhang, B. Yang, K. Li, D. Hou, C. Zhao, J. Wang, Electrospun porous poly(tetrafluoroethylene-co-hexafluoropropylene-co-vinylidene fluoride) membranes for membrane distillation, RSC Adv. 7 (2017) 56183–56193.
[30] S. Divya, J. Hemalatha, Study on the enhancement of ferroelectric β phase in P (VDF-HFP) films under heating and poling conditions, Eur. Polym. J. 88 (2017) 136–147.
[31] L.N. Sim, S.R. Majid, A.K. Arof, FTIR studies of PEMA/PVdF-HFP blend polymer electrolyte system incorporated with $LiCF_3SO_3$ salt, Vib. Spectrosc. 58 (2012) 57–66.
[32] U.R. Farooqui, A.L. Ahmad, N.A. Hamin, Effect of polyaniline (PAni) on Poly(vinylidene fluoride-co-hexaflouro propylene) (PVDF-co-HFP) polymer electrolyte membrane prepared by breath figure method, Polym. Test. 60 (2017) 124–131.
[33] S. Sedaghat, F. Golbaz, In situ oxidative polymerization of aniline in the presence of manganese dioxide and preparation of polyaniline/MnO2 nanocomposite, J. Nanostruct. Chem. 3 (2013) 65.
[34] P. Jain, S. Varshney, S. Srivastava, Site-specific functionalization for chemical speciation of Cr(III) and Cr(VI) using polyaniline impregnated nanocellulose composite: equilibrium, Kinect, and thermodynamic modeling, Appl. Water Sci. 7 (2017) 1827–1839.
[35] J. Qiu, F. Liu, S. Cheng, L. Zong, C. Zhu, C. Ling, A. Li, Recyclable nanocomposite of flowerlike MoS_2@hibrid acid-doped PAni immobilized on porous PAN nanofibers for the efficient removal of Cr(VI), ACS Sustain. Chem. Eng. 6 (2018) 447–456.
[36] X. Guo, G.F. Fei, H. Su, L.D. Zhang, High performance and reproducible polyaniline nanowire/tubes for removal of Cr(VI) in aqueous solution, J. Phys. Chem. C 115 (2015) 1608–1613.
[37] A.K. An, J. Guo, E.J. Lee, S. Jeong, Y. Zhao, Z. Wang, T. Leiknes, PDMS/PVDF-HFP hybrid electrospun membrane with superhydrophobic property and drop impact dynamics for dyeing wastewater treatment using membrane distillation, J. Membr. Sci. 525 (2017) 57–67.
[38] S.H. Hosseini, A. Mansourizadeh, Preparation of porous hydrophobic poly (vinylidene fluoride-co-hexafluoropropylene) hollow fiber membrane contactors for CO2 stripping, J. Taiwan Inst. Chem. Eng. 76 (2017) 156–166.
[39] B.S. Lalia, E.G. Burrieza, H.A. Arafat, R. Hashaikeh, Fabrication and characterization of polyvinylidenefluoride-co-hexafluoropropylene (PVDF-HFP) electrospun membranes for direct contact membrane distillation, J. Membr. Sci. 428 (2013) 104–115.
[40] Z. Liu, H. Wang, E. Wang, X. Zhang, R. Yuan, Y. Zhu, Superhydrophobic poly (vinylidene fluoride) membranes with controllable structure and tunable wettability prepared by one-step electrospinning, Polymer 82 (2016) 105–113.
[41] K. Yoon, B.S. Hsiao, B. Chu, Formation of functional polyethersulfone electrospun membrane for water purification by mixed solvent and oxidation processes, Polymer 50 (2009) 2893–2899.
[42] K.Y. Foo, B.H. Hameed, Insights into the modeling of adsorption isotherm systems, Chem. Eng. J. 156 (2010) 2–10.
[43] S. Babel, T.A. Kurniawan, Cr(VI) removal from synthetic wastewater using coconut shell charcoal and commercial activated carbon modified with oxidizing agents and/or chitosan, Chemosphere 54 (2004) 951–967.
[44] J. Geng, Y. Yin, Q. Liang, Z. Zhu, H. Luo, Polyethyleneimine cross-linked graphene oxide for removing hazardous hexavalent chromium: adsorption performance and mechanism, Chem. Eng. J. 361 (2019) 1497–1510.
[45] J. Wang, K. Pan, E.P. Giannelis, B. Cao, Polyacrylonitrile/polyaniline core/shell nanofiber mat for removal of hexavalent chromium from aqueous solution: mechanism and applications, RSC Adv. 3 (2013) 8978–8987.
[46] L. Li, Y. Li, C. Yang, Chemical filtration of Cr(VI) with electrospun chitosan nanofiber membranes, Carbohydr. Polym. 140 (2016) 299–307.
[47] T.S. Najim, A.L. Salim, Polyaniline nanofibers and nanocomposites: preparation, characterization, and application for Cr(VI) and phosphate ions removal from aqueous solution, Arab. J. Chem. 10 (2017) 3459–3467.
[48] M.I. Shariful, T. Sepehr, M. Mehrali, B.C. Ang, M.A. Amalina, Adsorption capacity of heavy metals by chitosan/poly(ethylene oxide)/activated carbon electrospun nanofibrous membrane, J. Appl. Polym. Sci. 7 (2018) 135.
[49] D. Duranoglu, A.W. Trochimczuk, U. Beker, Kinetics and thermodynamics of hexavalent chromium adsorption onto activated carbon derived from acrylonitrile-divinylbenzene copolymer, Chem. Eng. J. 187 (2012) 193–202.
[50] M. Kazemi, M. Jahanshahi, M. Peyravi, Hexavalent chromium removal by multilayer membrane assisted by photocatalytic couple nanoparticle from both permeate and retentate, J. Hazard. Mater. 344 (2018) 12–22.
[51] J.A.A. Casarrubias, M.R.C. Diaz, J.C. Martinez, J.V. Arenaz, F.V.C. Dominguez, Chromium adsorption into a microporous resin based on vinylpyridine-divinylbenzene copolymer: thermodynamics, kinetics, and process dynamic in the fixed bed column, Adsorption 24 (2018) 105–120.
[52] P. Baruah, D. Mahanta, Adsorption and reduction: combined effect of polyaniline emeraldine salt for removal of Cr(VI) from aqueous medium, Bull. Mater. Sci. 39 (2016) 875–882.
[53] T. Wang, L. Zhang, C. Li, W. Yang, T. Song, C. Tang, Y. Meng, S. Dai, H. Wang, L. Chai, J. Luo, Synthesis of core-shell magnetic Fe_3O_4@poly(m-phenylenediamine) particles for chromium reduction and adsorption, Environ. Sci. Technol. 49 (2015) 5654–5662.
[54] J. Wu, K. Chen, X. Tan, M. Fang, X. Hu, Z. Tang, X. Wang, Core-shell CMNP@PDAP nanocomposites for simultaneous removal of chromium and arsenic, Chem. Eng. J. 349 (2018) 481–490.
[55] H. Zhu, J. Wu, M. Fang, L. Tan, C. Chen, N.S. Alharbi, T. Hayat, X. Tan, Synthesis of a core-shell magnetic Fe_3O_4-NH_2@PmPD nanocomposite for efficient removal of Cr (VI) from aqueous media, RSC Adv. 7 (2017) 36231–36241.
[56] V. Jousseaume, M. Morsli, A. Bonnet, XPS study of aged polyaniline films, J. Appl. Polym. Sci. 90 (2003) 3730–3736.
[57] L. Ge, C. Han, J. Liu, In situ synthesis and enhanced visible light photocatalytic activities of novel PAni-g-C3N4 composite photocatalysts, J. Mater. Chem. 22 (2012) 11843–11850.
[58] J. Ding, L. Pu, Y. Wang, B. Wu, A. Yu, X. Zhang, B. Pan, Q. Zhang, G. Gao, Adsorption and reduction of Cr(VI) together with Cr(III) sequestration by bolyaniline confined in pores of polystyrene beads, Environ. Sci. Technol. 55 (2018) 12602–12611.